Heritage Science

RESEARCH

Open Access

Artificial weathering of rock types bearing petroglyphs from Murujuga, Western Australia

Jolam T. Neumann[1*], John L. Black[2], Stéphane Hœrlé[3,4], Benjamin W. Smith[2,4], Ron Watkins[2], Markus Lagos[1], Alexander Ziegler[5] and Thorsten Geisler[1]

Abstract

Murujuga in Western Australia has the largest concentration of ancient rock engravings (petroglyphs) in the world. However, the Murujuga rock art is potentially threatened by local industrial air pollution, in particular by acid rain, but unambiguous scientific evidence is still missing. Here, we report on results of an accelerated weathering experiment, simulating Murujuga weather and climate conditions that was designed and performed to test whether the expected small changes in chemical, mineralogical, and physical characteristics of the rock surface can be detected and reliably quantified by various analytical means. Locally acquired Murujuga granophyre and gabbro samples with natural varnish were artificially weathered for up to four months in a climate chamber under conditions that simulated 2 years of natural weathering. Mineralogical, chemical, and physical changes were qualitatively monitored by X-ray diffraction and confocal Raman spectroscopy, and quantified by colorimetry, portable X-ray fluorescence spectrometry, and micro-computed tomography. In addition, artificial rainwater that was sprinkled over the rock samples was collected and analysed by inductively-coupled plasma mass spectrometry. The results show significant chemical and physical changes of the surfaces of the rock varnish after 1 month of artificial weathering. The analytical results demonstrate that it is possible to quantitatively monitor small changes caused by the weathering of gabbro and granophyre. Therefore, such a semi-actualistic experimental approach, when carefully designed, potentially allows testing the hypothesis that the weathering rate of the Murujuga petroglyphs is increased by local industrial air pollution. Further experimental work is currently under way.

Keywords: Murujuga, Petroglyphs, Varnish, Patina, Artificial weathering, Rock engravings, Industrial emissions

Introduction

Murujuga (also known as Burrup Peninsula) is part of the Dampier Archipelago in the north of Western Australia and is well known for its Aboriginal rock art. It is estimated that the archipelago contains over one million petroglyphs that range in age of production from possibly 40000 years up to European occupation of the region in the 1860s [1]. Many of the petroglyphs depict geometric forms and representations of people, while others depict different aquatic and terrestrial animals. Some petroglyphs are large, measuring over one metre in length and width, whereas others are small and intricate (Fig. 1b–d, f) [2]. A sequence of changes in art styles and composition over time is illustrated by Mulvaney [3, 4]. Since July 2007, 44% of the peninsula has been listed as a National Heritage Place and, in January 2020, it was inscribed on the tentative list for UNESCO World Heritage sites [5].

The Murujuga bedrock mainly consists of granophyre, gabbro, and basalts formed in the Neoarchean [6]. Depending on the rock grain size, the commonly weathered surface is more or less smoothed. A huge diversity of surfaces and rock shapes are engraved at Murujuga. There are almost no granophyre or gabbro areas where petroglyphs are totally absent. There are significant

*Correspondence: jolam@uni-bonn.de

[1] Institute of Geoscience, Division of Geochemistry and Petrology, University of Bonn, Meckenheimer Allee 169, 53115 Bonn, Germany
Full list of author information is available at the end of the article

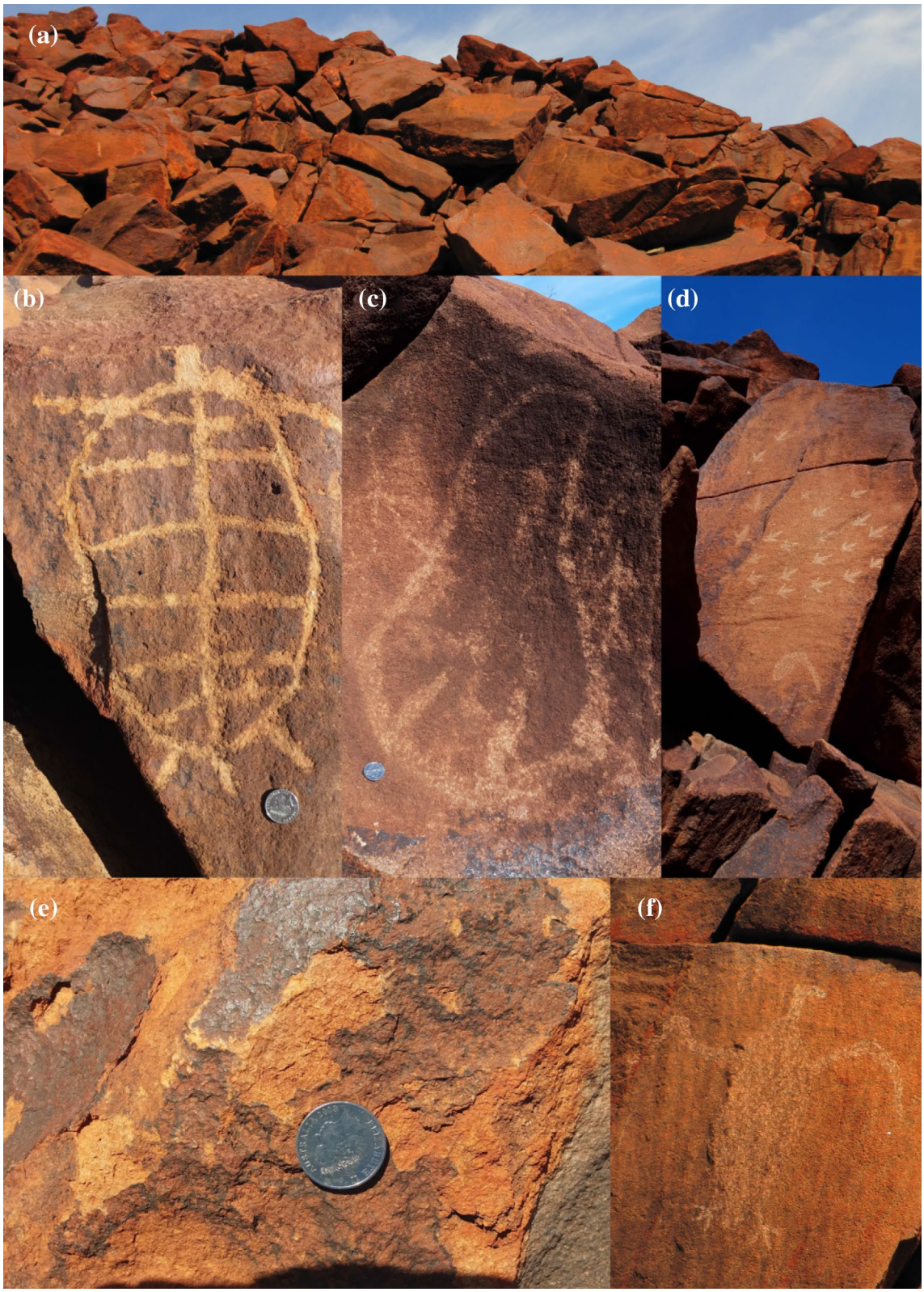

Fig. 1 Rock art on Murujuga. The dark red surface is the rock varnish. The varnish was removed by the artists to uncover the lighter weathered rind of the rock to produce the petroglyphs. **a** Landscape on Murujuga with intact rock varnish. **b**, **c** ,**d** ,**f** Different petroglyphs. **e** Effect of physical weathering of an unworked surface, causing varnish flaking off, which would have destroyed any petroglyphs that might have been present

concentrations of petroglyphs in all rocky ephemeral stream valleys, especially around the point at which these valleys join more open plains [4]. The granophyre and gabbro are characterised by a thin, whitish, weathered layer of about one centimetre maximum thickness that is covered by a 1 to 200 µm thick outer darker red-brown layer, known as the patina or rock varnish, that consists of about 25 wt.% Fe and Mn oxides and 75 wt.% clay minerals (mostly montmorillonite and kaolinite) [1, 7]. Other studies report about 70% clay minerals and 25% Fe and Mn oxides and hydroxides [8], while analyses from rock varnish from different sources all over the world revealed that 10 to 18 wt.% of the varnish are Fe and 10 to 19 wt.% are Mn oxides [9]. The varnish is necessary for the rock art, which is produced by a range of techniques, including scratching and pecking into the dark rock varnish to expose the whitish weathering rind underneath. Due to the colour difference between the dark rock varnish and the underlying lighter weathered zone of the rock, the petroglyphs are rich in contrast, particularly when freshly made (Fig. 1b).

Rock varnish forms under similar climatic conditions all over the world, but how it forms remains controversial. In particular, the high Mn concentration of the surface varnish, which is 50 to 300 times higher than in the unweathered rock, indicates the existence of a Mn source and enrichment process [10]. Some models for varnish formation are based on abiotic processes [11], whereas others consider biotic processes to be central to their origin [10]. There is evidence for the presence of an unusually aerobic microbial ecosystem on the surface of the rock varnish from Murujuga [7, 12, 13], including photosynthetic cyanobacteria that can enrich manganese and iron [12]. Recent evidence shows that various cyanobacteria accumulate extraordinary amounts of intracellular Mn that is used by the bacteria as a catalytic antioxidant necessary to cope with the substantial oxidative stress present in a desert environment [14].

Under pre-industry conditions, new growth of varnish counterbalanced the natural decay of the varnish due to weathering; thus, the colour contrast between the varnish and the carved parts of the petroglyphs was reduced over time with the varnish growing over the exposed lighter weathering rind [8]. Some of the older petroglyphs at Murujuga are fully patinated and show no colour contrast with the surface of their parent rock. Nonetheless, they remain visible due to their textural and topographical contrast with the parent rock surface. Given the age proposed for some of the petroglyphs it is clear that natural weathering processes in this landscape must be extremely slow and that the natural lifespan of petroglyphs here is exceptional, projected to persist for 60,000 years [15]. However, there remains debate about whether the degradation of the petroglyphs has been accelerated by local industrial emissions since the beginning of industrial development on the peninsula in the second half of the twentieth century [16–22]. The observation of accelerated degradation would not be surprising, considering that in its National Pollutant Inventory the Australian Government lists at least 320 t of ammonia, nearly 9000 of nitrogen oxides, and more than 300 t of sulphur dioxide that were released into the air by the industrial complexes on the peninsula in 2019 alone [23]. Smith et al. showed, using observations from the Copernicus satellites, that nitrogen dioxide was widely distributed across the archipelago, and highly concentrated over the industrial area [24]. It is known that nitrogen oxides released into the air lead to acid rain [25] which could result in accelerated dissolution of the rock varnish on Murujuga and thus a faster decay of the petroglyphs [24]. Bednarik reported that the pH of natural rain in the Pilbara region of Western Australia was in the order of 6.8 prior to industrial development and reached values between 7.0 and 7.2 at Murujuga [18], which is essentially consistent with observed neutral pH values for rain in the Arizona rangelands, where desert varnish is notably widespread and no polluting industries were operating [26]. The pH of the rainwater in the township of Dampier dropped from these values in the 1960s to a mean value of about 4.6 for sites monitored on Murujuga in 2007 [27]. Because both the solubility of Fe and Mn oxides and their dissolution rate increase dramatically when pH is lowered [18, 28, 29], it is evident that ongoing industrial development could erase the petroglyphs if industrial emissions were to continue at the levels currently reported. The International Federation of Rock Art Organizations (IFRAO) has issued a warning that about a quarter of the rock art has already been destroyed by the industrial development and that the remaining art is heavily endangered due to acid rain [30].

These conclusions by IFRAO agree with the observations made by members of the local Aboriginal community on Murujuga, who have repeatedly warned about the endangerment of their cultural heritage [31]. However, so far, no unequivocal scientific evidence has been reported to support their concern. Many of the scientific studies published to date have been poorly designed and/or conducted so that their results remain highly controversial [18–22, 24, 32]. In particular, a recent publication by MacLeod and Fish concludes that industrial emissions have no adverse impact on the petroglyphs [32]. Smith et al. claim that this conclusion is based on unsubstantiated, misleading and scientifically unsound data [24]. Therefore, there is an urgent need to design and perform studies that can ultimately answer the question as to whether industrial emissions

are leading to accelerated weathering of the rock varnish. Such studies must deliver robust and reliable data that can be used to support governmental decisions about further industrial developments on Murujuga and assist in the development of strategies to protect the rock art. Field studies can potentially deliver important data to address the underlying scientific questions, but are highly influenced by several uncontrollable parameters, such as the exposure of a petroglyph to sun, wind, and rain, and it is thus very difficult to quantify the time-dependence of the degradation of the rock art. Also, monitoring of reference samples unaffected by any industrial emissions is necessary to quantify the level of natural weathering, but in the field, it is almost impossible to ensure the same conditions for all samples in different locations. Extreme weather events such as storms and tropical cyclones may also have a significant impact on the results from different sampling sites. It follows that a semi-actualistic, carefully designed weathering experiment could be an approach to reliably and confidently test the hypothesis that accelerated weathering of the rock art may occur due to local industrial emissions [33, 34] However, with such an experimental approach, it is unclear whether the analytical techniques currently available are able to quantify with sufficient precision the expected small mineralogical, chemical, and physical changes associated with the weathering reactions within laboratory time scales.

Here, we report on a proof-of-concept study in which Murujuga granophyre and gabbro rock samples bearing surface rock varnish were artificially weathered under controlled accelerated conditions [35]. The samples were placed in a climate chamber that controlled temperature and humidity, and were regularly sprinkled with artificial rainwater to mimic Murujuga precipitation rates, while solar thermal radiation was simulated with infrared lamps. One sample of granophyre and two samples of gabbro were removed from the test chamber after one, three, and four months of artificial weathering and then analysed by a variety of (micro-)analytical techniques, including micro-computed tomography (μCT), confocal Raman spectroscopy, X-ray diffraction (XRD), portable X-ray fluorescence (PXRF), and colorimetry, to test whether the chemical, mineralogical and physical changes caused by artificial weathering could be visualised, detected and, importantly, quantified with sufficient precision. At the end of the experiment, the precipitation solution collected during a single artificial rain event was analysed for Fe, Mn, Si, Al, Ca, and Na by inductively-coupled plasma mass spectrometry (ICP-MS) to test whether dissolution of surface minerals can be detected already after one rain fall event. This proof-of-concept study forms the basis for further studies to determine the weathering of Murujuga petroglyphs under controlled and accelerated conditions.

Experimental procedures and analytical methods

Experimental procedure

Samples

With the consent of Aboriginal Traditional Owners, pieces of rock used for experimentation with an intact and flat rock varnish surface were collected on Murujuga and comprise both dominant bedrock lithologies, i.e. gabbro and granophyre. Nine rock cubes (three from a granophyre and six from a gabbro sample) each with a volume of about 1 cm^3 and a surface that is as flat as possible were cut from the collected rocks using a rock saw with a 300 μm thick blade (Fig. 2). Gabbro is more coarsely grained than granophyre, with a rough and irregular dark brown to grey varnish (Fig. 2a). The granophyre is fine grained and the rock varnish has a reddish-brown colour (Fig. 2b). Mineral grains cannot be seen with the naked eye (Fig. 2b).

The gabbro samples consist mainly of plagioclase with crystals up to 1 mm in diameter. Most crystals are deformed and altered. Other major components are biotite, hornblende, and pyroxene. The gabbro also contains a few quartz crystals. Petrographic thin sections that were cut show that the granophyre mainly consists of quartz, plagioclase, and alkali feldspar. Needle-shaped and compact pyroxene crystals appear as mafic components. The chemical composition of the gabbro and granophyre samples was determined by portable PXRF and is compared in Table 1 with an analysis of each rock type from Geoscience Australia [1]. The Fe and Al contents of the sample used in this study are significantly higher than in the samples analysed by Geoscience Australia, although care was taken to avoid contamination of the bulk material with the varnish.

The mineralogical composition of the rock varnish of both rock types was determined by XRD and Raman spectroscopy and is also given in Table 1. For more information about the mineralogy, petrography, and chemistry of both rock types the reader is referred to Donaldson [1].

Experimental details

A Weisstechnik (model SB11/300/40) climate chamber was used that allows running temperature and humidity cycles within the necessary range. Solar thermal radiation was simulated with two infrared lamps with a power of 40 W each. The radiated area was 15 cm in diameter and the duration of radiation was calculated with the data from Table 2 (solar exposure energy). Precipitation was simulated using nozzles connected to a water pump and

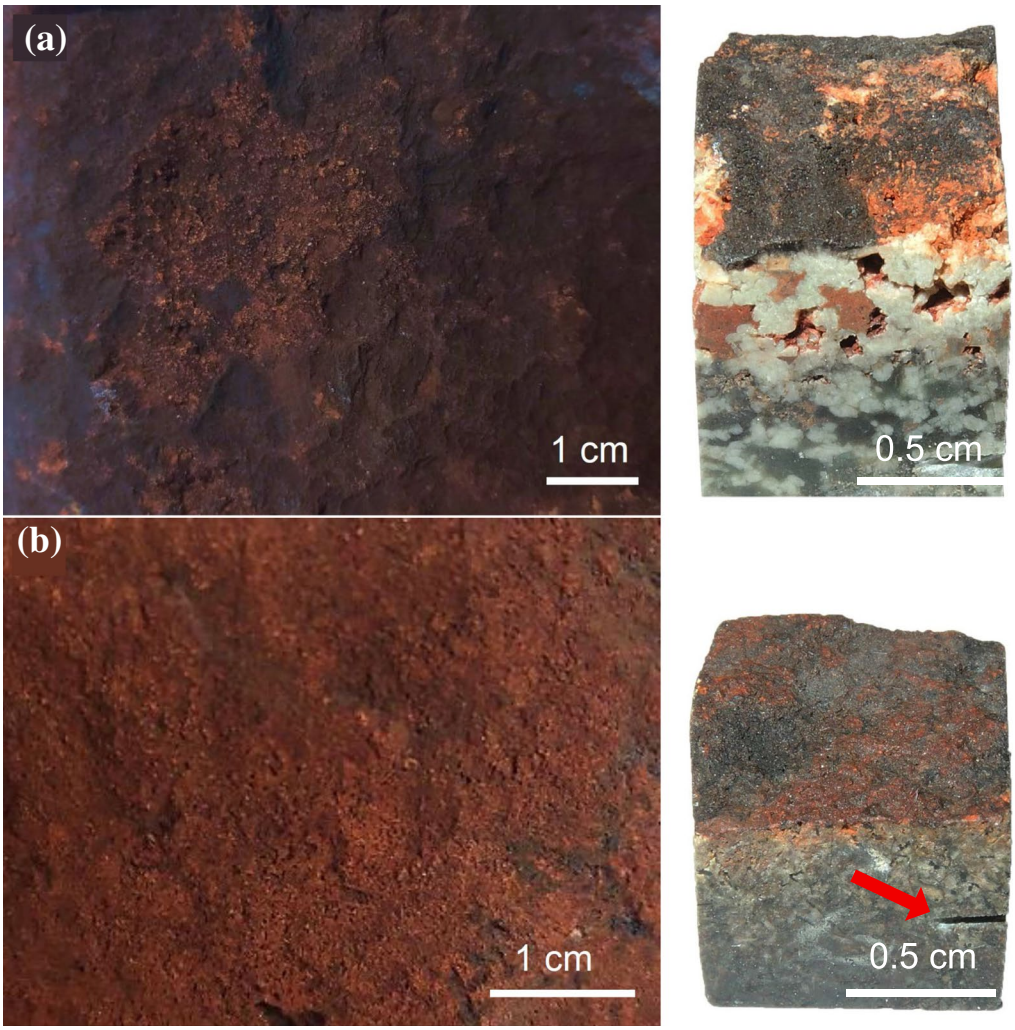

Fig. 2 Photographs of the rock varnish on the surface of **a** the gabbro and **b** the granophyre samples from Murujuga. Cubes from **a** the more coarsely grained gabbro and **b** finely grained granophyre. The weathered rind of the gabbro is more porous compared to the weathered rind of the granophyre. The recesses on the lower right-hand side (red arrow) have been engraved to facilitate repositioning of the cubes for all analytical measurements performed

placed inside the climate chamber (Fig. 3). The pump and nozzles generate 1 mm of precipitation per minute. The experimental design included an infrared thermometer that was mounted on an acrylic glass frame and facilitated monitoring surface temperature of the rock samples with an accuracy of ± 0.5 °C (Fig. 3).

Rainwater was simulated by mixing de-mineralised water with an acidic solution, containing nitric and sulphuric acid. The pH-value of the water was adjusted to 4.8 ± 0.1 to be comparable to the acid rain on Murujuga [27]. The sample tray was placed on a net to drain off the artificial rainwater. In order to prevent the acidic rainwater from reaching the water cycle of the climate chamber, the whole frame was placed in a plastic tub. The climate simulation was accelerated by a factor of 6. This means one daily cycle that is simulated lasts 4 h. During the experiment a total of 2 years were simulated during the 4 months (Fig. 4).

The rock cubes remained in the climate chamber for one, three, or four months. For each time step, three cubes were removed, two gabbro and one granophyre (Fig. 4). Before the cubes were placed in the climate chamber the varnish surface was analysed by XRD, Raman spectroscopy, PXRF, µCT, and colorimetry. After the sample cubes were removed from the climate chamber, all analytical measurements were repeated in the same way and on the same spot to observe possible surface changes.

In addition, after all other measurements were completed, a granophyre and two gabbro samples, which had been artificially weathered for four months, were

Table 1 Chemical bulk rock and varnish analyses of samples used in this study compared to rock analyses by Geosciences Australia and published by Donaldson [1] and the mineral paragenesis of the varnish and bulk rock, determined by Raman spectroscopy, XRD, and from thin sections, respectively. PRXF was used for bulk rock and varnish analysis

Element	Gabbro			Granophyre		
	Bulk rock		Varnish	Bulk rock		Varnish
	Donaldson [1]	This study		Donaldson [1]	This study	
SiO_2	52.10	50.25	34.50	71.44	70.23	32.71
Al_2O_3	16.72	17.03	20.95	12.40	12.35	11.23
Fe_2O_3	2.37	8.86	16.64	2.34	4.69	11.36
MgO	7.70	7.55	n.a	1.08	1.82	n.a
CaO	11.12	10.95	2.66	1.66	0.69	0.93
Na_2O	1.79	n.a	n.a	3.56	n.a	n.a
K_2O	0.69	0.45	0.79	3.75	2.57	1.16
TiO_2	0.48	0.48	0.74	0.52	0.54	0.71
MnO	0.15	0.15	6.42	0.08	0.07	2.60

Mineralogy	Gabbro (this study)	Granophyre (this study)
Varnish	Hematite, magnetite, albite, clinochlore, clinozoisite, quartz, anatase, and organic matter	Hematite, magnetite, albite, microcline, kaolinite, quartz, anatase, and calcite
Bulk rock	Plagioclase, quartz, mica, pyroxene, hornblende, and ore minerals	Alkali feldspar, pyroxene (incl. needle-like pyroxene), fine matrix of quartz, feldspar, and ore minerals

n.a. not analysed

Table 2 Climate data from Murujuga that was used for the simulation in the climate chamber

Simulated Month	Temperature [36] max. [°C]	Temperature [36] min. [°C]	Humidity [37] max. [%]	Humidity [37] min. [%]	Precipitation [36] [mm]	Solar exposure per day [36] [kWh/m^2]
Jan	40.3	29.0	98	13	48	7.47
Feb	40.1	28.9	94	12	75	7.08
Mar	40.1	28.4	99	17	47	6.58
Apr	37.5	26.0	99	12	17	5.67
May	33.5	21.9	89	11	27	4.72
Jun	29.5	19.4	99	13	36	4.22
Jul	29.2	17.8	95	15	14	4.69
Aug	31.1	18.0	98	10	4	5.67
Sep	34.7	19.8	97	10	0	6.64
Oct	38.7	24.4	95	12	0	7.47
Nov	39.6	25.8	93	12	0	7.94
Dec	40.3	28.1	92	10	14	7.86

sprinkled with artificial rain for 15 min a total of five times. The sprinkled samples had an initial surface temperature of 60 ± 1 °C. The artificial rainwater that was in contact with the rock varnish was collected and analysed by ICP-MS to test whether measurable quantities of different elements, in particular Fe and Mn, can be detected as a result of surface dissolution. Small Teflon© containers were used to collect the artificial rainwater, which consist of a bowl to collect the water with a small base for the sample in the middle (Fig. 5b). The bowls were closed with a cover that has an opening in the middle. Two of these containers were thoroughly cleaned and simultaneously placed in the climate chamber. One of these containers was not filled with a rock sample to collect a blank sample from each run.

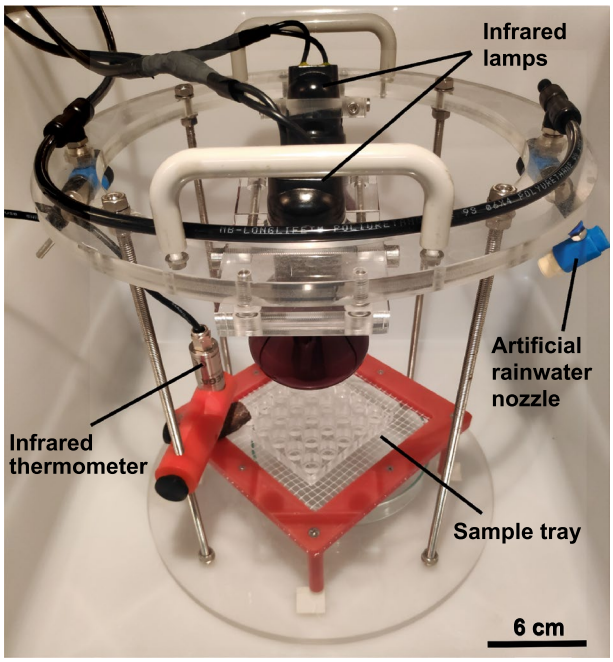

Fig. 3 Sample tray with infrared thermometer, artificial rainwater nozzles, and infrared lamps to simulate solar radiation, which was placed in a climate chamber

Climate data and simulation

The aim was to create weathering conditions that as closely as possible imitated the conditions on Murujuga. The climate on Murujuga is semi-arid with about 300 mm precipitation per year. Between August and November, the average precipitation is nearly zero. During the summer (December to February) the temperatures regularly reach more than 40 °C and do not fall below 20 to 25 °C at night. Most of the annual precipitation falls from February to June. During the winter the temperature can reach 30 °C during the day and rarely falls below 15 °C [36]. The minimum and maximum temperatures have been 6.9 and 48.2 °C over the last 26 years, respectively [36]. The surface temperatures on the rocks exceed the ambient temperatures due to solar radiation. For the weathering experiment, the monthly decile 9 maximum and minimum temperatures were chosen. The decile 9 value was calculated by assembling all temperatures for a month and dividing them into ten groups from highest to lowest. Decile 9 was the highest value of the ninth group, or the lowest value in the second group. This means the highest and lowest ten percent of the measurements were excluded [36]. The decile 9 values were considered to realistically represent daily temperature range on Murujuga for each month of the year, because they exclude rare extreme weather conditions.

The mean monthly precipitation on Murujuga over a time period of 47 years was used to simulate rainfall [36]. Unfortunately, the Australian Bureau of Meteorology does not record the humidity on Murujuga. However, a private weather station located in Karratha, 15 km south of Murujuga measured humidity for one entire year with monthly maximum and minimum values [37] that were approximated in the weathering experiment (Table 2). However, because of the limited ability of the climate chamber to control the humidity as fast as the temperature, the minimum humidity that was reached during the experiment was about 20%. The maximum was nearly 100%, and was always reached after the precipitation events.

To simulate the precipitation rates during the experiment, the samples were irrigated once every day, which equals every sixth day in the simulation. The duration of the irrigation depended on the monthly precipitation and ranged between 15 min of rain (February, Table 2) and no rain at all (September to November, Table 2). To simulate heating and cooling of the rocks by solar radiation, the infrared lamps were switched on for 1:35 (June, Table 2) to 2:58 h (November, Table 2) within four hours of a simulated day. The simulated ambient temperatures in the chamber ranged from 40.3 °C in January to 17.8 °C in July (Table 2). The measured rock surface temperatures reached up to 47.5 °C in January and were always approximately 3 to 7 °C higher than the temperatures in the climate chamber. The minimum surface temperatures of the samples were equal to the minimum ambient temperatures.

Within one day of real time, we simulated six Murujuga days. The temperature and humidity reached their maximum and minimum values every four hours and

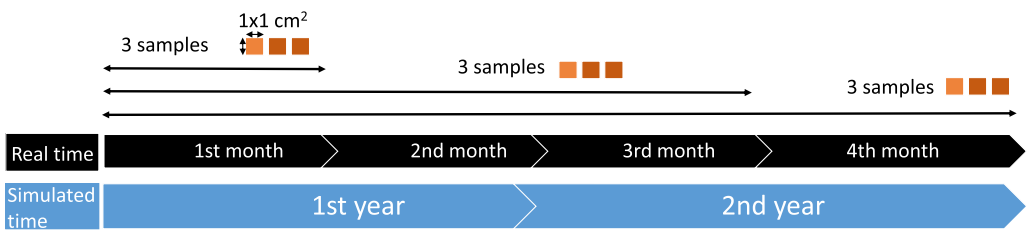

Fig. 4 Time sketch of the experimental procedure over 4 months, with six Murujuga climate days being simulated in a single day in real time

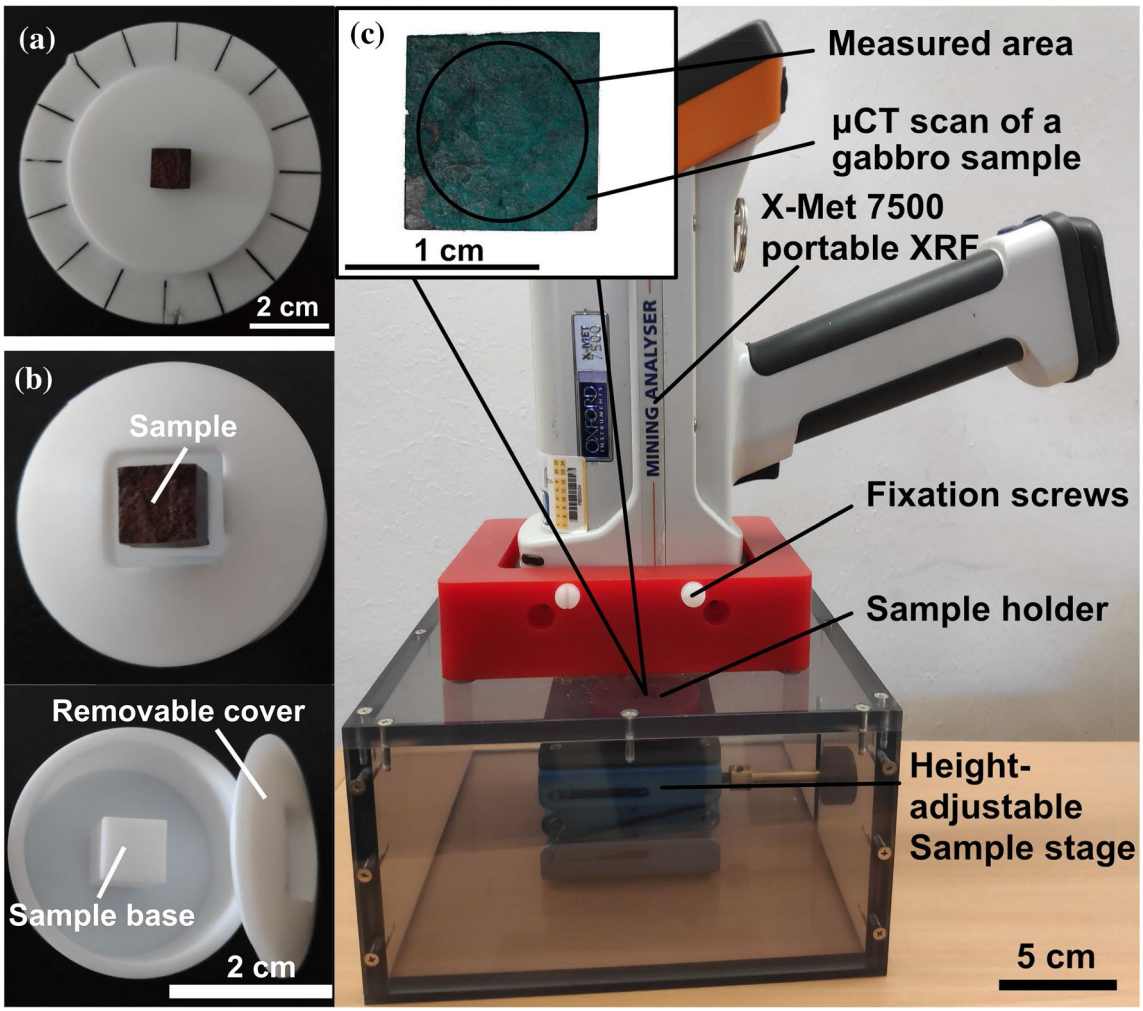

Fig. 5 Custom made analytical and experimental equipment. **a** Teflon© plate used for the colour measurements with a granophyre sample positioned in the centre. The markings on the outer ring were used to turn the chromameter by the same angle during each measurement. **b** Teflon© containers used to collect water samples during the artificial sprinkling experiment. The containers have a removable cover with a hole in the middle and a small base in the middle for the rock samples. **c** Holder for the PXRF used to ensure a reproducible positioning of the samples for every measurement. The holder consists of an acrylic glass case with a height adjustable sample stage on which the samples can be fixed. The PXRF is held in position by four plastic screws on the sides. The inset in the upper left corner shows the measured area (spot size) of the PXRF, measured with an X-ray film, on a superimposed µCT scan of a gabbro sample

developed contrarily. The solar exposure was simulated simultaneously with the maximum temperature. Irrigation was set to take place at the beginning of every daily cycle.

Analytical methods

The mineralogical, chemical, and physical state of the samples before and after the weathering experiment was monitored by PXRF, confocal Raman spectroscopy, µCT, XRD, and colorimetry. A statistically rigorous analytical data evaluation was performed and all uncertainties are given at the 95% confidence level. Student's *t*-test was used to determine if two values from two sets of data were significantly different from each other (i.e., the error of probability α is smaller than 0.05 or 5%).

Colorimetry

A portable "CR-410 Chroma Meter" from Konica Minolta was used for surface colour measurements that is based on a wide-area illumination with a 0° viewing angle (specular component included). The measured area of the chromameter had a diameter of 50 mm and was illuminated by a pulsed xenon lamp [38]. The instrument was equipped with six silicon photo-diodes (three

for measurements and three for lighting control) that are filtered for the primary perception of red, green, and blue light. The CIELAB (L*a*b*) colour space was used, because the colour difference can be calculated easily and previous reports on varnish colour used the same colour space [19, 22].

The standard deviation of ΔE*, given by the manufacturer of the colorimeter for measurements that are calibrated with a standard ceramic calibration plate, is within ± 0.07. In our case, however, the measured circular area has a diameter of 50 mm and the cubes' surface only measured approx. 10×10 mm^2. Hence, the samples only made up about 5% of the measured area and the colour that was measured does not represent the real colour of the sample surface. Moreover, the surface was rough and uneven, causing light to be irregularly reflected and dispersed from the surface, which strongly affected the reproducibility of the measurements even if the sample was only slightly misoriented. We therefore developed a special measurement approach and empirically evaluated the reproducibility. The samples were positioned on a round polished Teflon© plate that was also used to calibrate the instrument. The plate was carefully handled, stored, and regularly cleaned with ethanol to avoid any errors due to dust or fingerprints on the plate. The Teflon© plate was marked in the centre and had 16 marks on the outer ring to position the chromameter (Fig. 5a). These markings were used to rotate the chromameter 16 times through the same angle while taking a measurement at each orientation. Each cube was measured four times before and after the weathering experiment, so that a single value of L*, a*, and b* represents the average of 64 individual measurements from which the standard deviation of the mean was estimated. Between each of the four measurements, the instrument was re-calibrated using the Teflon© plate. To further test the reproducibility of the colour measurements and to detect possible sources of errors, one reference cube, that was stored under ambient dry conditions, was always measured at the beginning of each new sample measurement. The reproducibility of the ΔE* and ΔL* value was estimated from the multiple measurements to be between 12 and 8% for ΔE* and ΔL* values between 0.08 and 0.40 and between -0.05 and 0.33, respectively.

X-ray fluorescence spectrometry

The element composition of the gabbro and granophyre samples were quantitatively determined by XRF using an AXIOS 3 kV wavelength-dispersive XRF spectrometer (Malvern PANalytical). Major element analyses were carried out according to DIN EN 15309 on fused glass beads that were prepared by diluting the sample with di-lithium tetraborate flux agent and melting the mixture under a Bunsen flame in platinum crucibles. For the determination of the loss of ignition (LOI), about 5 g of dried powder was placed in an Al_2O_3 crucible and heated for one hour at 1100 °C in a furnace. The sample powder was weighed before and after heating with a precision of ± 0.0002 g on an analytical balance. Standardless major element analyses were performed using the *IQ*+ program (©PANalytical). Major element X-ray intensities were corrected for matrix effects by a refined fundamental algorithm between concentration and characteristic X-ray intensities that is based on Sherman's equation [39] and implemented in *IQ*+. The reproducibility was tested on multiple sample preparations and analyses of international standard samples and was found to be better than ± 2% for major (and better than ± 5% for trace) elements. The accuracy of the measurements was regularly checked by participating in ring tests of the GeoPT-International Association of Geoanalysts. Using standardless analysis, the detection limits for light major elements Na, Mg, Al, Si, and P are in the order of 100 ppm and for K, Ca, Ti, Mn, and Fe between 1 and 10 ppm.

Since the samples have a rough varnish surface and could not correctly be fitted in the sample holder of the desktop XRF, an X-MET 7500 PXRF from Oxford Instruments was used to analyse the surface of the cubes before and after the experiment. The X-MET 7500 includes a 45 kV X-ray tube as radiation source and a large area silicon-drift X-ray detector. All elements from magnesium to uranium can be detected and quantified with detection limits down to the lower ppm level that is comparable to benchtop instruments [40]. In order to ensure that exactly the same spot on the sample surface was measured before and after the experiment with the same sample-beam-detector geometry, a special instrument holder was built (Fig. 5c). The holder consisted of a bracket for the PXRF and a height-adjustable sample stage. The stage had a particular bracket to fix the sample, allowing change in the position of the sample only along the vertical axis. The PXRF has a proximity sensor that measured the distance to the sample. With this sensor, it was also possible to reproduce the distance between sample surface and PXRF detector. The spot size of the PXRF measurement, that was determined with an X-ray film, was smaller than the geometric sample surface and has a round shape with a radius of about 5 mm (Fig. 5c). With such a spot shape and size, the outer edges of the samples were not analysed.

All sample surfaces were measured ten times and the integration time was 60 s per measurement. The measured X-ray intensities were corrected by the instrument using a fundamental matrix correction algorithm that is based on Sherman's equation [39], basically allowing standardless quantification. However, for complex

matrices, the measurements from the PXRF can be very inaccurate. To account for this, the pressed pellets that were produced from the bulk rock and varnish samples were used as standards to correct the PXRF data. The comparison of the results led to a linear dependency with correlation coefficients of > 0.93 between the measured concentrations of the two devices. As we are primarily interested in relative changes, possible systematic errors affecting the accuracy have negligible effects on our results. To estimate the reproducibility of the measuring procedure, the samples were taken out and repositioned after each measurement. From these measurements, the reproducibility of the analyses was empirically estimated to be in the order of $\pm 0.27, \pm 0.13, \pm 0.08, \pm 1.1$, and ± 1.0 wt.% for Fe, Mn, Ca, Si, and Al, respectively, and involves the X-ray counting errors and any excess error that results from sample repositioning. In addition, two pristine sample surfaces were measured before every analytical session as reference. These samples were expected to show no chemical difference over time. We obtained apparent chemical differences of 0.63 ± 3.53, 2.78 ± 1.61, 1.31 ± 2.84, -1.53 ± 4.14, and -2.59 ± 6.52 wt.% for Fe, Mn, Ca, Si, and Al, respectively, which are, with the exception of Mn, all zero within the limit of the estimated errors (given at the 95% confidence level).

X-ray diffraction (XRD)

XRD measurements of the sample surface were carried out using a Siemens "D500" diffractometer. The diffractometer consists of a θ-2θ-goniometer with a graphite single-crystal monochromator, a scintillation detector, and a Siemens Kristalloflex 710D X-ray generator, operating with 40 kV and 40 mA. The detector aperture was set to 0.2 mm. Measurements were taken between 4° and 70° 2θ with steps of 0.02° 2θ. The acquisition time of each 2θ step was 20 s, leading to a total acquisition time of about 8 h per sample. The measured diffraction spectra were analysed with the *EVA*© (Bruker AXS, 2019) and *TOPAS*© (Bruker AXS, 2014) software to qualitatively determine the surface mineralogy and to identify possible mineralogical changes during artificial weathering. Therefore, again all samples were measured before and after the experiment.

Raman spectroscopy

Hyperspectral Raman spectroscopic imaging was carried out with two different Raman spectrometers. All images taken from the sample surface before the experiment were acquired with a "LabRAM HR800" and a "LabRAM HR Evolution UV" Raman spectrometer from Horiba Scientific using a 532.09 nm Nd:YAG laser and a 632.81 nm He–Ne laser as excitation sources with a laser power at sample surface of less than 5 mW. The same area of 200×200 µm^2 was imaged on each sample before and after the experiment in order to investigate possible mineralogical changes on the surface. All images were taken in the point-by-point mode with a step size of 4 µm. The chosen step size was a compromise between image recording time and the size of the analysed surface area that should be large enough to be representative for the sample surface.

Each image thus consists of 2600 pixels, each of which represents one single Raman measurement. The location reproducibility of the imaged area was estimated to be within ± 1 µm. All measurements were carried out with a 50 × long working distance objective with a numerical aperture of 0.5 [41], yielding a lateral resolution (spot size) in the order of 2 µm. A high precision piezo translator and feedback signal to automatically track and adjust the laser focus on the sample surface was used as the autofocus system. The spectrometer entrance slit was set to 100 and the confocal hole to 1000 µm. A grating with 600 grooves/mm was used and the Raman spectrum at each point (pixel) was collected for 20 to 26 s, respectively, depending on the signal-to-noise ratio obtained from the respective sample. Spectrometer drift during long-time measurements was corrected using known emission lines of a neon lamp as reference. With these settings, the spectral resolution in the frequency region of interest was about 3.5 and 3.3 cm^{-1} with 532 and 632 nm excitation, respectively. Phase identification was performed with the help of the RRUFF Raman spectral database [42]. The colour-coded hyperspectral images were generated from the array of Raman spectra using the classical least-square fitting method that is described in detail in Hauke et al. [41]. Data treatment and evaluation was performed with the *LabSpec 6*© software from Horiba Scientific [43].

Micro-computed tomography

To visualise and quantify morphological changes such as crack formation or physical and chemical degradation, all samples were analysed using a Bruker "SkyScan1272" X-ray µCT scanner before and after the weathering experiment. The source voltage was set to 90 kV and the isotropic voxel resolution was limited to 6 µm due to equipment constraints. The samples were rotated with a step size of 0.3° using an exposure time for every step of 1785 ms.

Following reconstruction, each µCT scan did result in a stack of tomographic images that were further analysed using different data processing tools. The first reconstruction was carried out with the *NRecon*© software from Bruker. To render the reconstructed image stacks comparable to each other, all samples were reconstructed in three dimensions using the same grey-scale limits (lighter

grey shades indicate denser material). The reconstructed image stacks were further analysed and compared using the software *Dragonfly*© Ver. 2020.2.0.941 [44]. Here, scans of a given sample taken before and after the experiment were loaded and a 3D registration was performed. For this registration, *Dragonfly*© compared and superimposed these two models. Following the registration, structural differences between both models became visible and a region of interest (ROI) was determined. The volume inside the ROI was then calculated using *Dragonfly*© in order to quantify the occurred changes. However, because the results from this volume analysis were not sufficiently reliable, another approach was chosen: screenshots from the top side of the superimposed 3D models were analysed and the area that had changed was visualised and calculated using *FIJI* [45]. This method resulted in reliable quantitative results.

Inductively-coupled plasma mass spectrometry

The concentrations of selected elements (Fe, Mn, Si, Al, Al, Ca, and Na) in the rainwater samples that were collected during artificial irrigation of the samples were measured by Sector Field ICP-MS using an "Element 2/XR" instrument from Thermo Fisher Scientific. The sample solution volume ranged from 5 to 10 ml per sample. After sampling, the solutions were stabilized adding 10 µl of concentrated, ultrapure nitric acid per millilitre sample volume to each sample. Prior to the measurements each sample was twice diluted by adding 2 vol.% ultra-pure nitric acid. Each sample dilution was measured in duplicate and all measurements were performed in medium mass resolution of about 4,000 to minimize signal contribution from potentially interfering species.

Element concentrations were determined based on the signal intensities and a five-point linear calibration for each element using five different dilutions of a multi-element stock solution that was prepared using a mixture of the ICP multi-element standard solution Certipur VI from Merck and a Si mono-element standard solution from SCP Science. To validate the calibration and test the accuracy, two certified reference materials (lake water TM-26.4 from Environment Canada in fourfold dilution for Fe and Mn and SPS-SW2 in tenfold and 40-fold dilution for Si, Al, Ca, Na, and Mg) were measured as unknowns. For each element the certified concentration values could be reproduced within a 95% confidence interval. Throughout the whole analytical sequence, the mean value of both replicate sample measurements was used as the concentration value except for one blank sample, because one of both measurements failed. The quantification limit calculated based on the tenfold standard deviation of the background intensities were 0.32, 0.006, 24.4, 1.2, 14, and 5 ppb for Fe, Mn, Si, Al, Ca, and Na respectively. Typical uncertainties (95% confidence level) were 3–14, 4–37, 7–17, 4–11, 4–18, and 4–20% for Fe, Mn, Si, Al, Ca, and Na, respectively.

Results

Colour changes

In general, the colour measurements showed statistically significant changes on all samples that were artificially weathered (Fig. 6a, b), which are for most of the samples significantly larger than the apparent colour and lightness change observed for the reference ($\Delta E^* = 0.024 \pm 0.004$, $\Delta L^* = 0.0009 \pm 0.0100$). The largest colour changes occurred on the gabbro surfaces that were artificially weathered for 3 months ($\Delta E^* = 0.40 \pm 0.02$). Overall, the surface colour of gabbro samples changed more than that of the granophyre samples. It is also noted that the ΔE^* and ΔL^* values of most samples were lower after 4 months than after one and three months of weathering (Fig. 6a, b). The change in ΔL^* of one gabbro and one granophyre surface was even negative after 4 months, i.e., the sample became darker during the experiment (Fig. 6b). Statistically, the average ΔE^* values are all significantly higher than from the unweathered reference samples, which is clear evidence that the surface colour has changed as a result of artificial weathering. We also note that the changed area, calculated from µCT data, correlates well with the calculated ΔE^*, especially for the granophyre samples (Fig. 6d).

Textural and morphological changes

Textural and morphological changes were studied by µCT. Figure 7 shows the images from all superimposed before-after 3D scans. The images from the gabbro surfaces show that material was lost during the experiment. Most material loss occurred on the edges and corners on the top side of the cubes (Fig. 7). The gabbro cubes that had been artificially weathered for 3 months showed major material loss at the edges. The cubes that have been artificially weathered for 1 month longer showed the least morphological changes (Fig. 7), i.e., there was no clear correlation with the duration of the experiment (Fig. 6c). The 3D models of the granophyre samples are darker than those of the gabbro samples, because they are denser and more finely grained, and show small white spots all over the samples. These spots are anatase crystals that were identified by Raman spectroscopy (Fig. 8). Visibly, the superimposed models of the granophyre cubes do not show any significant differences (Fig. 7).

To quantify the morphological changes, the volume change was calculated from all µCT models. For this, a ROI with individual grey-scale borders was defined. When the same grey scale was used to define the ROIs, all models, except for the 4-months granophyre, showed

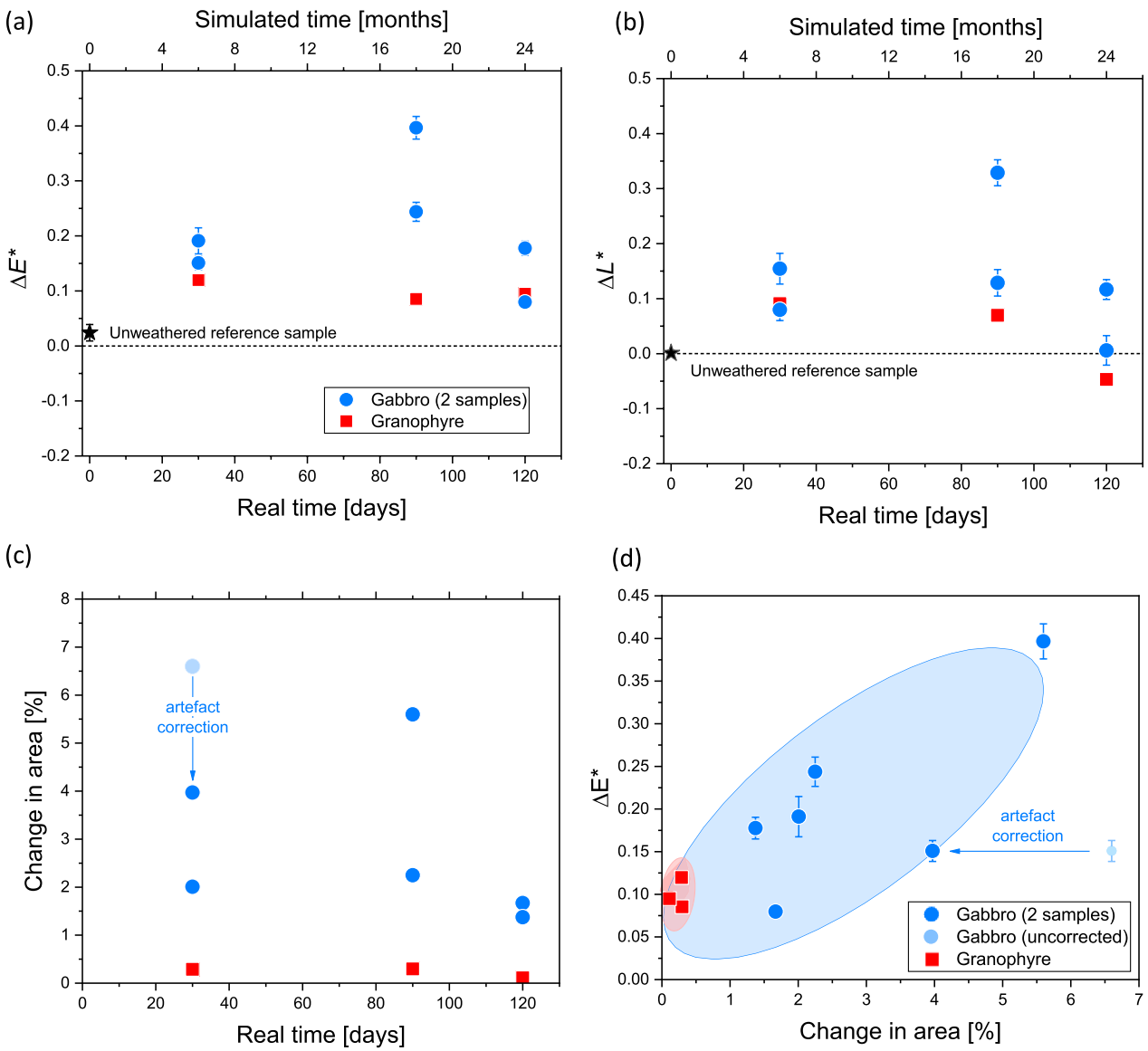

Fig. 6 **a** Colour change (ΔE*) and **b** change in brightness (ΔL*) of the samples surface as a function of the artificial weathering time. The error bars show the 95% confidence interval. If no error bar is visible, the error is within the symbol size. **c** The change of the varnish surface area as a function of artificial weathering time. The data from one 1-month gabbro sample had to be corrected due to a ring artefact that occurred during the µCT measurements. The topside view with the ring artefact is displayed next to the corrected measurement. Note that there is no clear correlation between detectable changes of the surface area and the artificial weathering time, but on average a significant weathering effect is noticeable. **d** A plot of ΔE* against the changed area with the 86 and 95% covariance ellipse for the granophyre and gabbro samples, respectively, showing a clear positive correlation between both parameter for the gabbro samples

loss of varnish in a range between 0.09 and 3.19 mm^3. The volume loss was also calculated using different grey scales for both models of the same cube. These grey scales were chosen by visual estimation. The results show an increased volume on two cubes and a decreased volume in a range of 0.05 to 5.82 mm^3 on the other cubes (Table 3). These results do not appear to be reliable as they indicate an increased volume for some cubes that clearly have visible losses. Instead, the topside view images from the superimposed cubes (Fig. 7) were analysed with *FIJI*. Using this image evaluation tool, it was possible to calculate the proportion of the surface that had changed. The calculated material loss ranges from 0.1 to 6.6% (Table 3) and correlates well with the visible losses from Fig. 7. One sample (gabbro, 1 month, 6.6% change), however, showed ring artefacts in some surface

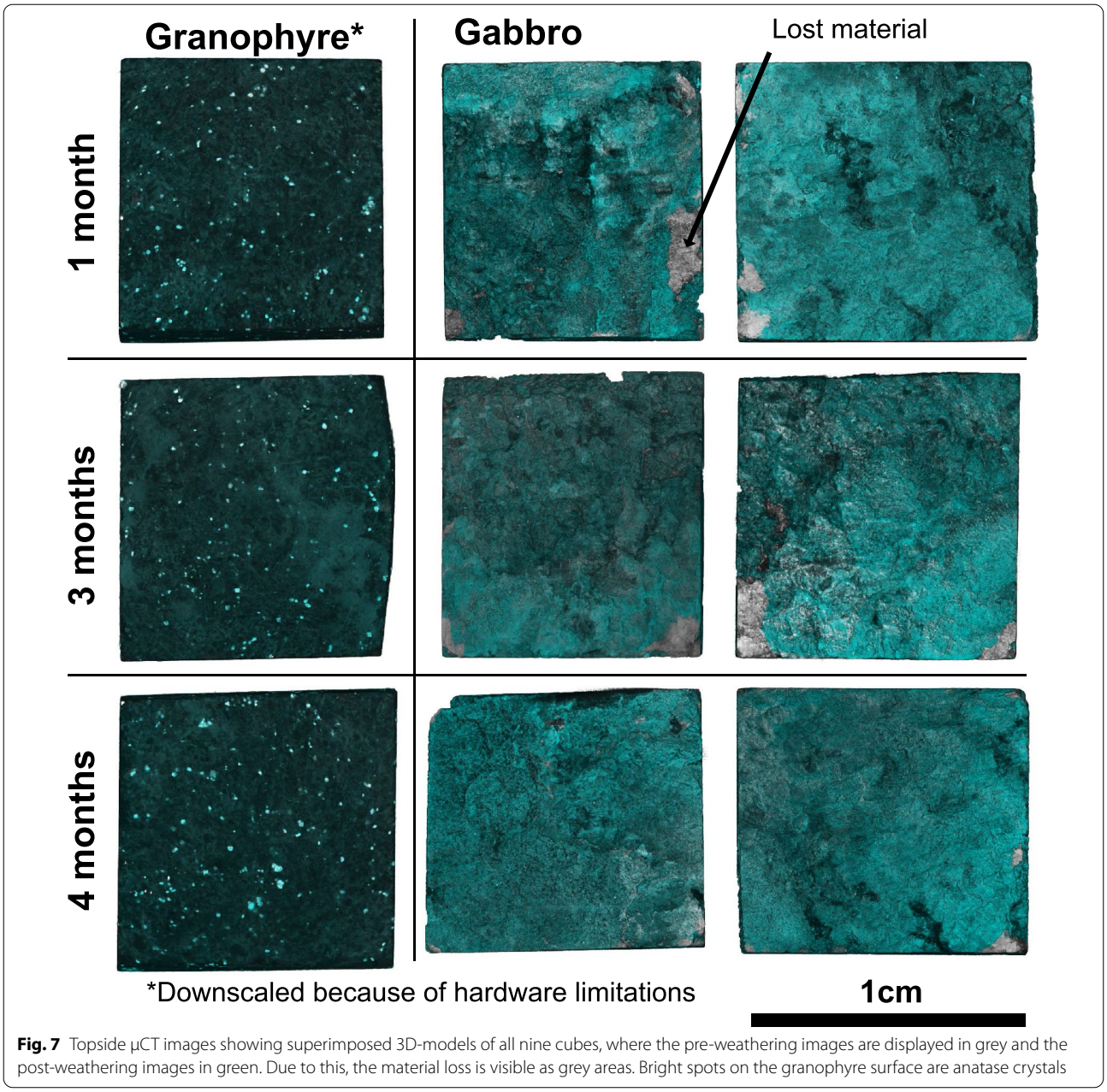

Fig. 7 Topside µCT images showing superimposed 3D-models of all nine cubes, where the pre-weathering images are displayed in grey and the post-weathering images in green. Due to this, the material loss is visible as grey areas. Bright spots on the granophyre surface are anatase crystals

sections, for which the data were corrected by visually excluding them from the calculations using the image editing program *Affinity*©.

Mineralogical changes

The Raman spectra from the different cubes, especially from the gabbro, before and after the experiment are characterized by a markedly different and partly strong fluorescence background with both laser excitations. Owing to this, most of the collected hyperspectral Raman maps and spectra could not reliably be compared to each other. Nevertheless, the Raman data could be used to identify the surface mineral paragenesis, including minor minerals such as calcite and anatase that were not detected by XRD. A direct comparison of the images taken before and after the experiment was only possible for one granophyre sample that was artificially weathered for 4 months (Fig. 9). In both hyperspectral Raman images quartz, iron oxides (mostly hematite and magnetite), anatase, and calcite were identified. When interpreting the images, it must be considered that even a small difference in positioning and laser focus can have a major

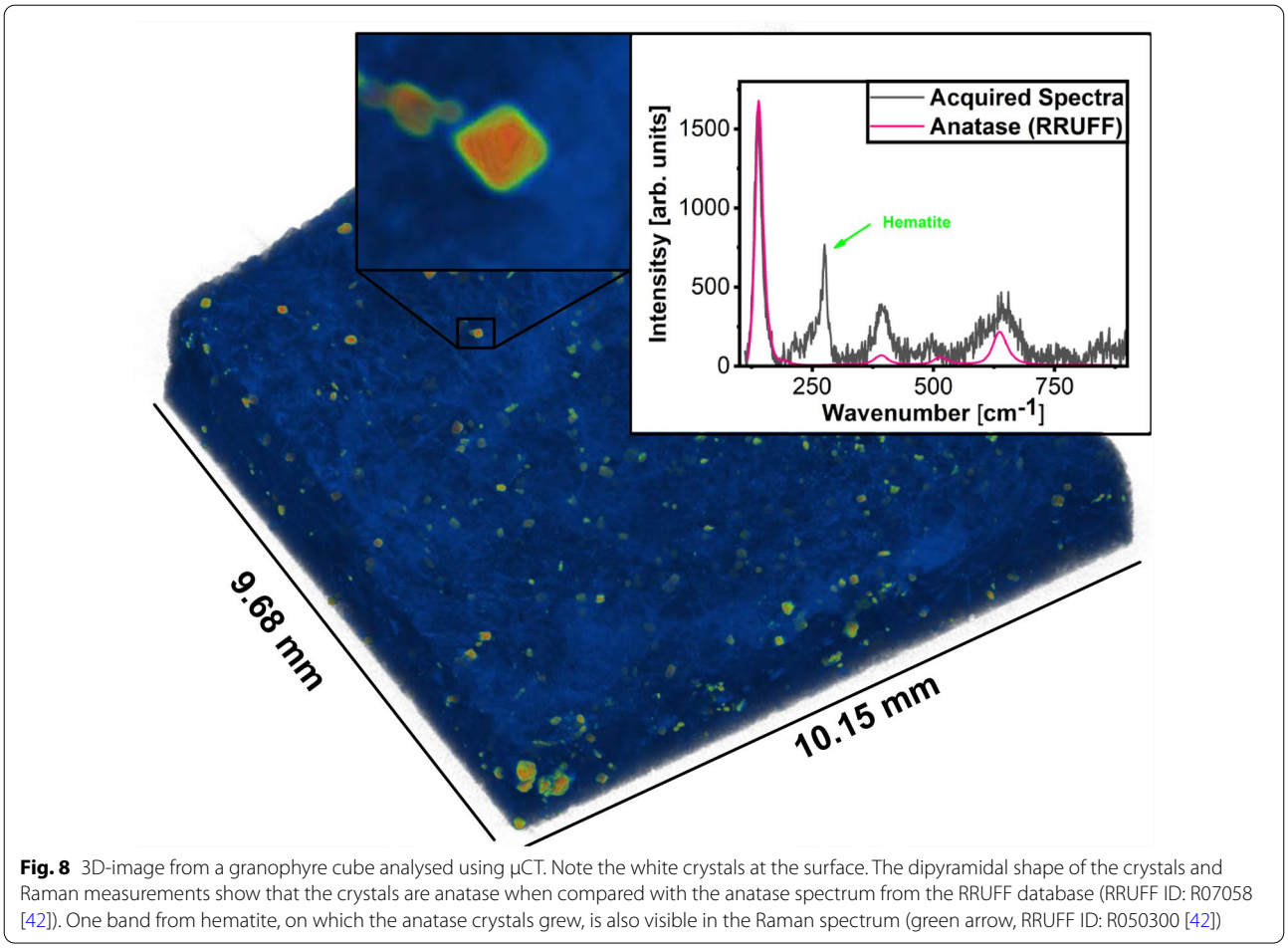

Fig. 8 3D-image from a granophyre cube analysed using µCT. Note the white crystals at the surface. The dipyramidal shape of the crystals and Raman measurements show that the crystals are anatase when compared with the anatase spectrum from the RRUFF database (RRUFF ID: R07058 [42]). One band from hematite, on which the anatase crystals grew, is also visible in the Raman spectrum (green arrow, RRUFF ID: R050300 [42])

Table 3 Calculated volume change of surface varnish for each sample for each time step

Sample	Time [months]	Volume change[1] [mm^3]	Volume change[2] [mm^3]	Change in area[3] [%]
Granophyre	1	− 3.19	− 5.82	0.29
Granophyre	3	− 1.45	− 4.19	0.30
Granophyre	4	1.31	− 0.05	0.11
Gabbro	1	− 2.11	− 8.90	6.60 (3.97[4])
Gabbro	1	− 1.00	− 7.11	2.01
Gabbro	3	− 0.09	1.17	2.25
Gabbro	3	− 3.17	− 4.79	5.60
Gabbro	4	− 0.04	0.32	1.67
Gabbro	4	0.96	− 0.67	1.37

[1] calculated with *Dragonfly*©, same grey scale used

[2] calculated with *Dragonfly*©, different grey scale used

[3] calculated with *FIJI*

[4] after artefact correction

impact on the Raman spectra of rough surfaces. In this context, the observed [differences are considered to be insignificant as they reflect slightly different x, *y*, *z* positions during both measurements and complex surface scattering effects. Nevertheless, we noted that the calcite crystals initially present on the surface are still detectable after four months of weathering, proving that they are at least not dissolved in the acidic rainwater that was used to simulate precipitation [46]. Only one calcite seems to have disappeared and a few anatase crystals seemed to have appeared in the images that were taken after the experiment, but actually calcite and anatase Raman signals could be detected in the Raman spectra from these areas on both images. They are not displayed in the image, because their Raman signals were overlapped by stronger signals from the surrounding iron oxides or quartz.

The hyperspectral Raman images from the gabbro samples that were taken before the artificial weathering

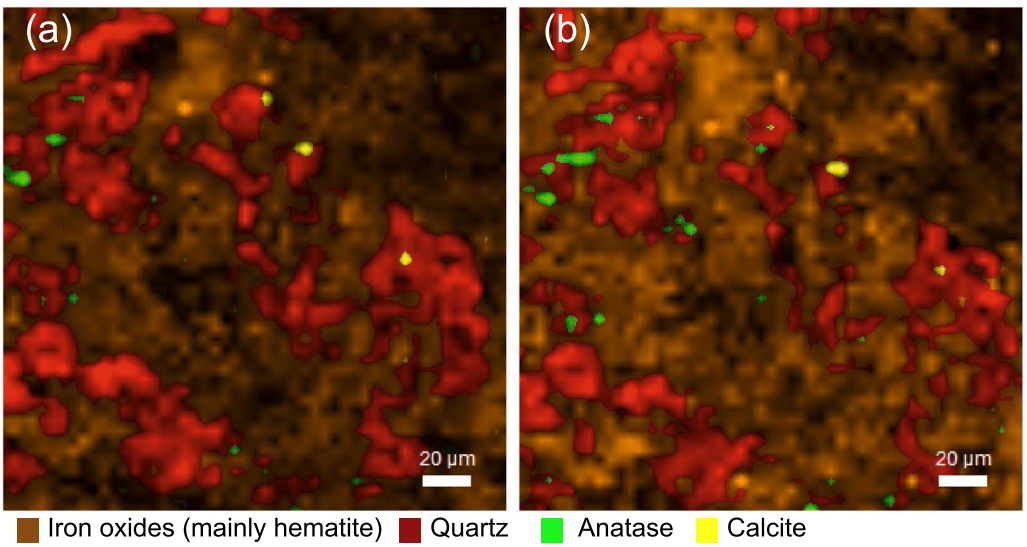

Fig. 9 Hyperspectral Raman image from an area **a** of a pristine granophyre cube and **b** after it was artificially weathered for 4 months. Both images show the distribution of quartz, iron oxides (mainly hematite and magnetite), anatase, and calcite. The images reveal no significant changes in mineralogy. One calcite crystal seems to have disappeared on image **b** and some anatase crystals seem to have formed, which can be attributed to repositioning errors, which are in the same order of magnitude as the crystal sizes. The 632.81 nm laser with 17 mW power (source power, < 5 mW on the sample surface) was used and each point was measured 2 times 10 s

experiment revealed the presence of organic and carbonaceous material. The carbonaceous material is characterised by two broad bands near 1340 and 1590 cm^{-1}, commonly called the D and G band, respectively (Fig. 10). In some areas these bands are overlain by a number of bands between 900 and 1800 cm^{-1} that can be assigned to vibrations of complex organic material. Noticeably, these bands are not detectable in the spectra from the same sample area that were recorded after the weathering experiment, but the carbonaceous phase is now unambiguously detectable by its characteristic D and G band. The very low laser power used for analysis (< 5 mW) precludes the formation of carbonaceous matter from organic material by local laser heating. It thus follows that the organic material must have been dissolved or washed away, whereas the carbonaceous material remained. The overall shape and relative intensities of both broad Raman bands indicate very immature carbonaceous matter and thus a low formation temperature (< 80 °C) [47], as is to be expected given that the varnish formed under surface temperatures.

Chemical changes

The percentage change in the Si, Al, Fe, and Mn concentration of the surface area in the centre of the samples as a function of weathering time is shown in Fig. 11. Si and Al can be viewed here as tracers of the silicate phases of the host rock and the kaolinite alteration layer under the desert varnish that, in turn, can be traced by Fe and Mn. All weathered samples show significant chemical surface changes, even those that were weathered for one month only. The relative change of Si and Al at the surface with time follows a positive linear trend for both rock types ($r^2 > 0.96$), with the granophyre samples showing a significantly larger rate of Si and Al loss from the surface than the gabbro samples ($\alpha < 0.05$). On the other hand, the Mn and Fe concentration of the gabbro surface decreased with weathering time. Assuming a linear time dependence, the slope is less than zero with probabilities of error of 0.03 and 0.29 for Mn and Fe, respectively. The element K, Ca, and Ti were also slightly depleted from the surface with increasing experimental weathering time (not shown here, but results are given in Table 4). However, the situation is different for the granophyre. Here, the Fe, Mn, K, Ca, and Ti surface concentrations of the 1-month granophyre sample stand out from the 3- and 4-months samples. These elements are relatively enriched at the surface after only 1 month of artificial weathering, while the surface concentrations of the 3- and 4-month samples are similar to those of the gabbro samples (Fig. 11).

Material loss during artificial irrigation

At the end of the experiment, the artificial rainwater that was sprinkled over the surface of two gabbro and one granophyre sample was collected and its Ca, Na, Si, Al, Fe, and Mn concentrations were measured by ICP-MS. Figure 12 shows the results in comparison to the concentrations in the blank rainwater sample. Since the samples

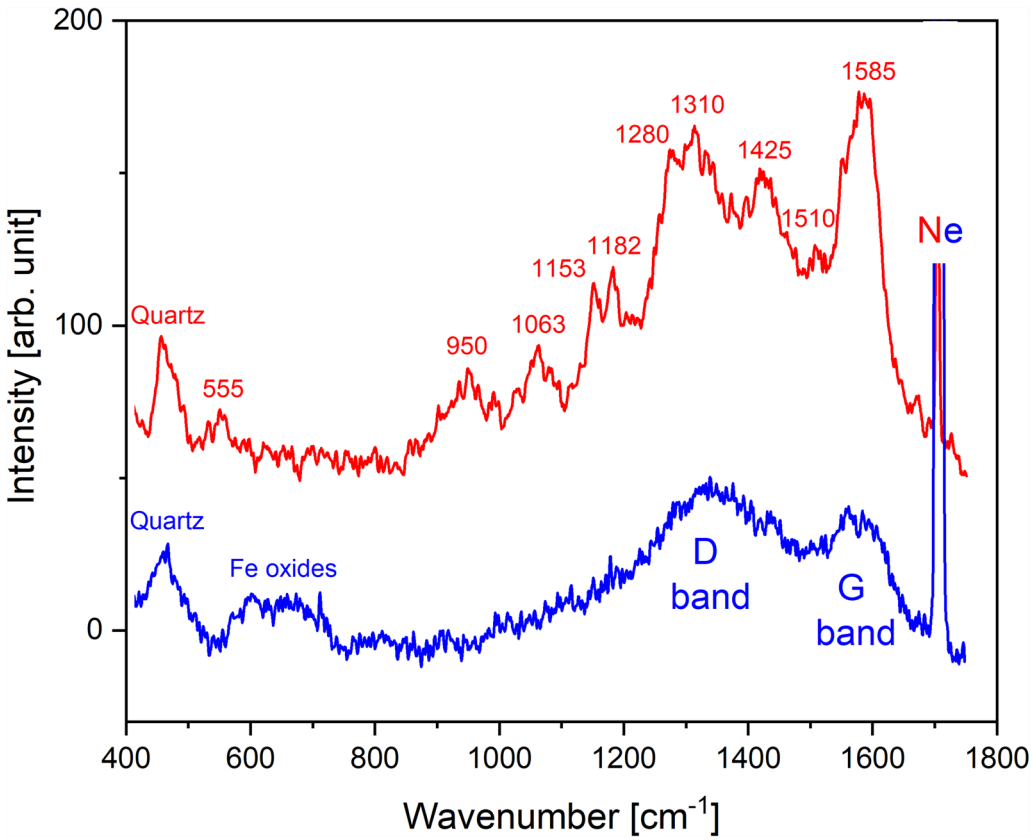

Fig. 10 Representative Raman spectra from the same location on a gabbro sample surface, measured before (red) and after (blue) 3 months of artificial weathering with a 532.09 nm laser. Beside the characteristic quartz band near 464 cm^{-1}, multiple bands occur in the frequency range between 900 and 1800 cm^{-1} which indicate the occurrence of complex organic material (all bands with frequency labels). These bands do not occur in the spectrum taken after artificial weathering (blue spectrum), where only the D- and G-band of carbonaceous matter are visible. These carbonaceous bands occur also in the red spectrum, but here are overlapped by organic bands. The sharp signal at 1707.06 cm^{-1} is a neon line that was used to correct for any spectrometer drift during long-time measurements

were already artificially weathered for 4 months, any dust, small particles, and organic relicts had already been washed from the surface.

All elements are significantly enriched in the water that was sprinkled over a sample surface, except for Fe and Si in one gabbro and granophyre sample, respectively. The absolute enrichment with respect to the blank water range between 0 ± 1 and 23 ± 1 ppb for Fe and between 8 ± 1 to 65 ± 4 ppb for Mn. Noticeably, the Mn concentration in the water that was rinsed over the gabbro samples was higher than in the water that was rinsed over the granophyre samples (Fig. 12). However, this can be explained by different Mn concentrations of the varnish surface. In fact, the normalisation of the solution concentrations to the surface concentrations analysed by PXRF does not show systematic differences between the gabbro and granophyre samples (Fig. 12).

Discussion

The main objective of this study was to evaluate with various analytical techniques whether it is principally possible to detect chemical, physical, and mineralogical weathering effects on the varnish surface within laboratory time scales under simulated Murujuga climatic conditions. In fact, significant changes in colour, chemical and physical properties of the rock surface were observed within 4 months, with one actual test day equalling six Murujuga days. The experimental results demonstrate the relative value of different analytical techniques to record weathering effects as a function of time with the used setups and settings. Raman spectrometry and XRD instruments provide qualitative mineralogical information, but could not be used to reliably quantify mineralogical changes. However, µCT, PXRF, and colorimetry enabled the quantification of chemical and physical changes with

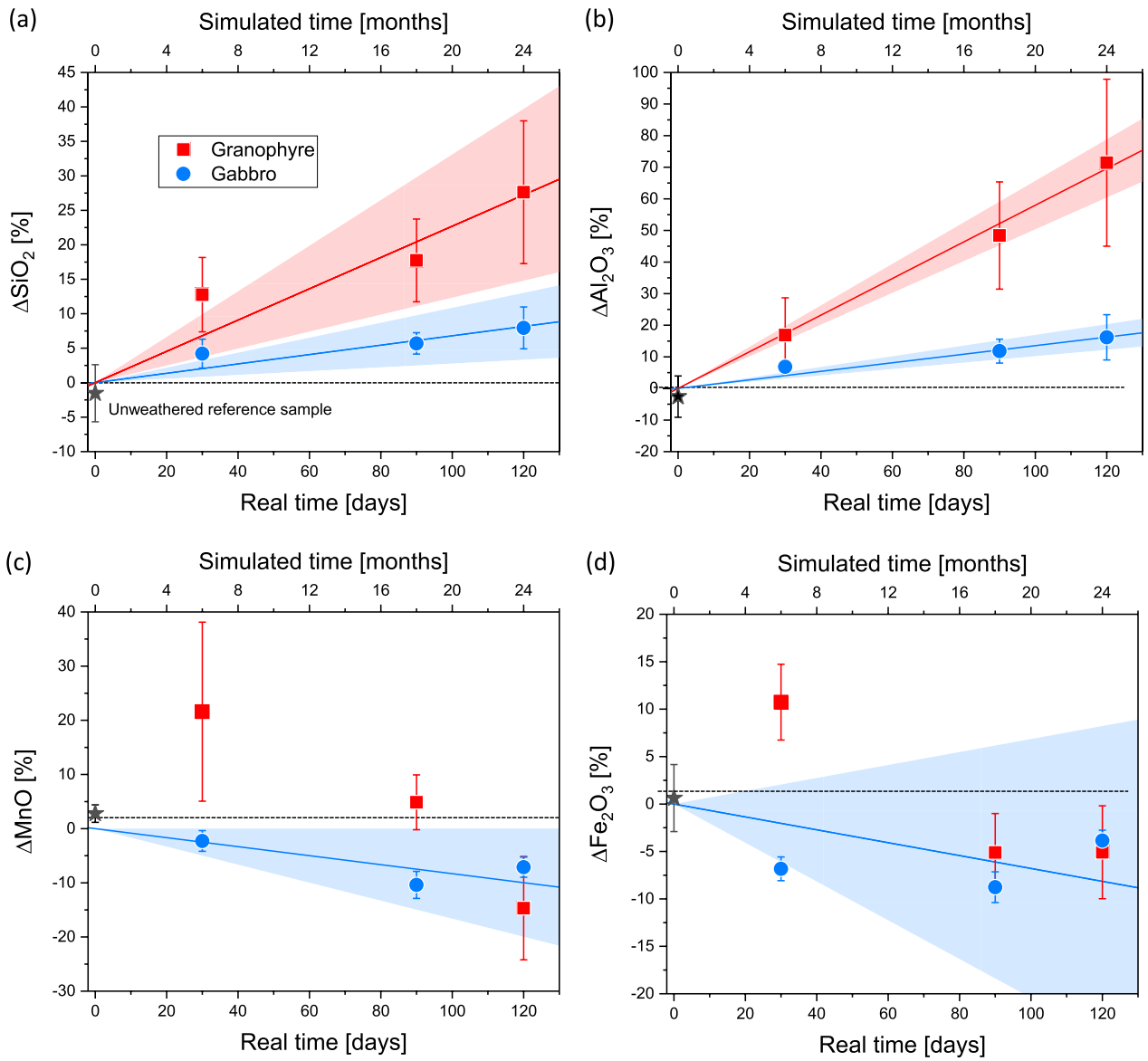

Fig. 11 Percentage change of different element concentrations on the sample of surface varnish with artificial weathering time. Least-squares regression lines are shown with the 95% confidence limit that is marked by coloured fields. The Fe and Mn data from the granophyre scatter erratically and are therefore not fitted with a function

Table 4 Summary of the difference in the element concentrations in the surface varnish with increasing artificial weathering time

Sample	Time [months]	Δ [wt.%]						
		SiO_2	Al_2O_3	Fe_2O_3	K_2O	CaO	TiO_2	MnO
Gabbro	1	4.2 ± 2.1	6.8 ± 2.1	− 6.8 ± 1.3	− 3.4 ± 1.5	− 14.9 ± 3.8	− 7.5 ± 1.9	− 2.3 ± 1.9
	3	5.7 ± 1.6	11.8 ± 3.8	− 8.77 ± 1.6	− 6.2 ± 1.6	− 8.70 ± 5.4	− 3.0 ± 4.0	− 10.39 ± 2.5
	4	8.0 ± 3.0	16.2 ± 7.2	− 3.9 ± 1.1	− 10.9 ± 1.2	− 22.4 ± 1.8	− 11.5 ± 3.8	− 7.1 ± 1.9
Granophyre	1	12.8 ± 5.4	16.9 ± 11.8	10.7 ± 4.0	17.4 ± 5.2	27.6 ± 2.1	9.1 ± 4.1	21.6 ± 16.5
	3	17.7 ± 6.0	48.4 ± 17.0	− 5.1 ± 4.1	− 7.0 ± 3.5	− 32.4 ± 1.6	− 13.9 ± 4.8	4.9 ± 5.1
	4	27.6 ± 10.4	71.4 ± 26.4	− 5.1 ± 4.9	− 9.6 ± 6.1	− 19.7 ± 3.2	− 7.5 ± 7.0	− 14.7 ± 9.5

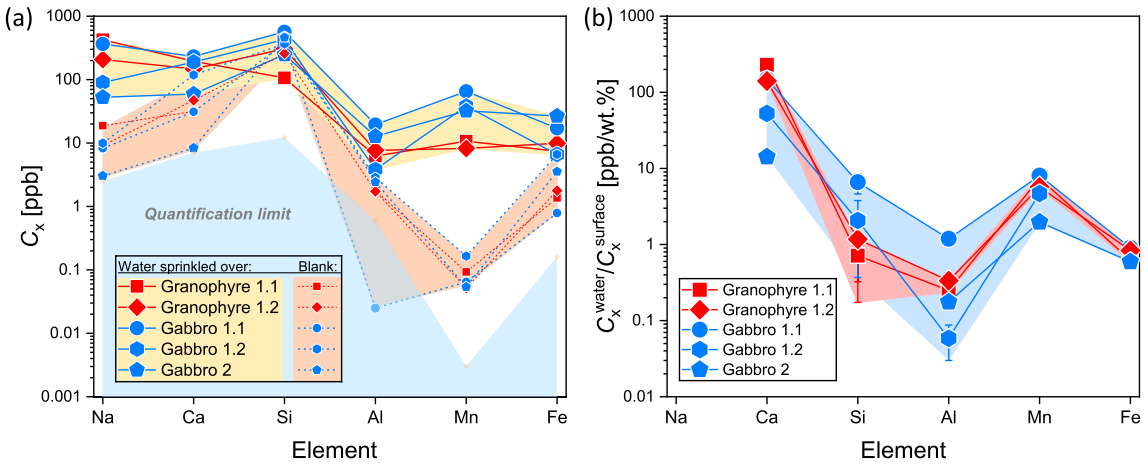

Fig. 12 **a** Spider plot of the element concentration in the blank artificial rainwater and in the artificial rainwater that was rinsed over the granophyre or gabbro samples. The detection limits are also plotted. **b** Spider plot of the change in element concentration normalised to the oxide concentration of the sample surface that was determined by PXRF (see Fig. 11). The value for Fe from gabbro 1.2 is not displayed, because it is slightly negative

weathering time, but particular care had to be taken to ensure that the same surface area was analysed before and after the experiment.

The surface roughness of the samples precludes quantitative treatment of the XRD data. This is because even slight, but unavoidable geometric sample-beam misalignments between the two measurements can have an influence on the relative diffraction intensities. In future, this problem may partly be overcome by using a sample spinning system that rotates the sample in phi axis during the measurement.

The colour change of the rock surface is considered to be one of the most important parameters for monitoring and quantifying the deterioration of the petroglyph [48]. However, previous studies using colour measurements on Murujuga rocks [19, 22] were not reliable or accurate enough due to inadequacies in experimental procedures and data evaluation [20, 48]. For instance, Markley et al. [22] carried out comprehensive colour measurements over a timespan of 10 years on different rock surface spots, but (i) changed the chromameter during data collection, (ii) did not evaluate the reproducibility of the measurements, (iii) did not assess the colour change over the whole timespan, and (iv) did not analyse the changes in brightness of their samples [20, 48]. In light of our results, the value of rock surface colour measurements is indeed highly questionable. We could clearly observe that even small differences in the sample position can have a major influence on the reproducibility. This is because the rough varnish surface scatters photons in different directions depending on their wavelength, which has an unpredictable effect on the colour measurement. We therefore collected multiple measurements under different orientations, which averaged out these scattering effects and provided an estimate of reproducibility. With this approach, the colour measurements revealed statistically significant changes in the ΔE^* and ΔL^* values of all artificially weathered samples. Such an observation is critical, because the petroglyphs are primarily visible due to the contrast between the dark rock varnish and the lighter coloured layer underneath. If the varnish is removed, the petroglyphs will disappear over time [18].

The observed correlation between colour change and changed area on the surface, quantified using the µCT data, suggests that part of the colour change is due to possible physical flaking and material loss, because most changes were visible along the edges of the porous gabbro samples. Owing to the limited voxel size of about 6 µm3 for the particular µCT scanner used, changes were only visible when relatively large pieces of material were removed, which can be expected for physical weathering effects. Mechanical disintegration of the varnish may be enhanced by thermal stress of the sample surface imposed by (artificial) solar heating and night-time cooling or moisture. Physical disintegration of the rock varnish is indeed also observed on Murujuga (Fig. 1e) [16]. Although no obvious signs of large-scale mechanical loss of mineral particles from the granophyre sample edges were detected using µCT, the average ΔE^* value of 0.10 ± 0.01 is evidence that some surface changes occurred, which is likely rather due to chemical processes (dissolution) than to physical effects. The ΔE^* value differences are not visible with the human eye, but are significantly ($\alpha < 0.05$)

higher than those obtained from the reference samples. The reason for the reversal of the colour and lightness change after 3-month weathering (Fig. 6a, b), which is not accompanied by a reversal in the chemical surface changes (Fig. 11), is as yet not fully understood. A possible explanation may be related to the small number of samples and to unpredictable mechanical saw effects, which may have affected the integrity of the bonds attaching the varnish to the underlying weathering rind, particularly on the gabbro samples. The observation that possible varnish flaking and material loss predominantly, but not exclusively, occurred along the edges of the gabbro samples supports this explanation and suggests that the effect of physical weathering in the experiment may be overestimated to some extent.

The results of the PXRF measurements reveal a linear increase of the surface Al and Si concentration and an overall significant decrease of Fe and Mn content with artificial weathering time. This indicates that Fe and Mn dissolved in the artificial rainwater and were washed away, while aluminosilicates and other rock-forming minerals were increasingly exposed to the analysed surface volume over time. It is noteworthy that the critical analysis depth of characteristic, i.e., element-specific X-rays, depends on their energy as well as the composition and density of the target material and thus varies for each element as well as at different surface sites. For Fe and Mn the analysis depth at the varnish surface is in the order of 100 to 300 µm, while for all other elements the analysis depth is well below 100 µm. Si and Al have a very similar analysis depth. Removal of any fine particles and organic compound from the rock surface during the irrigation process may have also contributed to the observed increases in rock surface Al and Si and the colour change. Unambiguous evidence for significant material loss due to chemical weathering through dissolution in rainwater, however, is given directly by ICP-MS analyses of the water that was sprinkled over the samples' surface at the end of the experiment when any loose material at the sample surface should have been washed off already. These measurements revealed a significant enrichment of Fe, Mn, Al, Ca, Si, and Na in the collected water of all samples (Fig. 12), which is evidence of a significant loss of material from the surface during a single, here 15 min long rainfall event, at least in slightly acidic water as used in our experiment and as is typical for the Murujuga peninsula ($pH = 4.8 \pm 0.1$) [27]. The consistency of the results from different samples suggests that the elemental concentrations in solution primarily reflect the dissolution of surface minerals and only marginally of rock-forming minerals from the vertical sides of the sample cubes (chemical weathering effect). Moreover, this consistency makes it very unlikely that fine particles washed off the surface after physically being detached from the underlying surface (physical weathering effect) were analysed.

Conclusion

Our results demonstrate that artificial weathering of the varnish surface of rock samples from Murujuga caused detectable physical and chemical changes, even within a simulated period of one month using slightly acidic rainwater with a similar composition to the rainwater on Murujuga. When correctly applied, colorimetry, PXRF, and µCT have been proven to be suitable analytical methods for the quantification of physical and chemical varnish surface changes. In addition, short time irrigation of an approximately 1 cm^2 varnish surface was sufficient to remove enough surface minerals for detection by ICP-MS analysis. All these methods have been shown to be suitable for detecting and quantifying the physical and chemical weathering effects under controlled weather and climate conditions.

Although our data clearly demonstrate that acidic rain has measurable effects on the varnish surface, including its colour and increased dissolution of Fe and Mn compounds, it should be stressed here that this does not necessarily mean that natural weathering of the petroglyphs is accelerated by anthropogenic pollution. Nevertheless, a recent analysis of photographs of twenty-six Murujuga petroglyphs from pre/early industrial development compared with recent photographs showed 50% changed over time, with the changes being attributed directly to industrial activity [49]. Modelling by Parsons and colleagues [50] shows that substantial deposition of nitrogen dioxide and nitric acid is concentrated over the industrial area of Murujuga, while deposition of sulphur dioxide is concentrated over the shipping lanes of the Murujuga coast, but extends to many locations containing rock art.

In future, further experiments are necessary in which, for instance, two representative sample groups should simultaneously be placed in a climate chamber, but irrigated with different waters. This would ensure that the weather and climate conditions are the same for both groups while only the composition of the rainwater differs. The natural rainwater compositions could be determined by sampling the rainwater on Murujuga as well as in a comparable region not affected by industrial emissions. The rock samples should be analysed once before the artificial weathering and after defined periods of time during the course of the weathering experiment. With such a semi-actualistic experimental approach, it should be possible to reliably quantify the difference between the weathering rate of the rock

varnish in contact with anthropogenically polluted and unpolluted natural rainwater under Murujuga climatic conditions. This statement is essentially in line with reliable and robust results obtained from other experimental studies with climate chambers to study weathering processes ([33, 34] and [49]). We thus hope to also encourage other researchers to design new experiments that study weathering of the rock varnish at Murujuga in order to obtain a more robust scientific understanding of the precise implications of industrial pollution. Such robust data will allow governmental and industrial decision makers to take the necessary steps concerning the protection of the extraordinary rock art heritage of Murujuga as well as other petroglyphs.

Abbreviations

µCT: Micro-computed tomography; XRF: X-ray fluorescence; PXRF: Portable X-ray fluorescence; XRD: X-ray diffraction; ICP-MS: Inductively-coupled plasma mass spectrometry; IFRAO: International Federation of Rock Art Organizations; ROI: Region of interest.

Acknowledgements

The authors thank the Murujuga Aboriginal Corporation for their support and for their permission to collect rock samples for analysis by this project. All rock samples were collected from locations that have been culturally cleared during industrial developments and that lie outside of Murujuga National Park. All rock samples came from locations already damaged by industrial development and that had no rock art or other registered sites of significance. The authors are committed to conducting research that inflicts no new damage to the rock art, archaeology, environments, living cultural values and viewsheds of Murujuga. This publication is produced as a part of the Murujuga Rock Art Conservation Project. This project, which analyses the effects of industrial pollution on Murujuga rock art, was funded by ordinary citizens who gave an amount in excess of AU$330,000 through crowd-funding. This extraordinary level of public support shows the extent of public concern that exists on this topic. We thank each of the many hundreds of people that supported this research. The views expressed in this paper are our own and may not reflect the views of those who have supported our research. We also thank Nils Jung and Hans Henning Friedrich from the University of Bonn for the preparation of the thin sections and the XRD measurements, and two anonymous reviewers for their valuable comments on an earlier draft of the manuscript. This is contribution No. 69 of the LA-ICPMS laboratory of the Institute of Geosciences, University of Bonn.

Author contributions

JN performed the Raman, XRF, colour measurements, and the weathering experiment in the climate chamber, prepared the samples, analysed the data and thin sections, and wrote the first draft of the manuscript. JB made contributions to the conception and revised the manuscript. SH made contributions to the conception and revised the manuscript. BS made contributions to the conception and revised the manuscript. RW made contributions to the conception and revised the manuscript. ML carried out the ICP-MS measurements and revised the manuscript. AZ carried out µCT scanning and revised the manuscript. TG designed the experimental program, helped to evaluate the data, and revised the manuscript. All authors read and approved the final manuscript.

Funding

Open Access funding enabled and organized by Projekt DEAL. This publication is produced as a part of the Murujuga Rock Art Conservation Project at the Centre for Rock Art Research & Management in the School of Social Sciences at the University of Western Australia. This project was funded by citizens through crowdfunding. None of the funding for the Murujuga Rock Art Conservation Project comes from industry or government. JN was financially supported by a PhD scholarship of the University of Bonn and a scholarship from the Rosa-Luxemburg-Foundation during his studies. The µCT system and Raman spectrometers were funded by the Deutsche Forschungsgemeinschaft (grant no. INST 217/849–1 FUGG, INST 217/653–1 FUGG, and INST 217/1010–1 FUGG, respectively).

Availability of data and materials

The datasets used and/or analysed during the current study are available from the corresponding author on reasonable request.

Declarations

Competing interests

JN—no competing interests. JB is an independent scientist and voluntary member of Friends of Australian Rock Art, which is an independent non-profit voluntary organisation established in 2006 to protect, preserve, and promote Australia's Aboriginal rock art, particularly the ancient petroglyphs of the Dampier Archipelago, including Murujuga. SH—no competing interests. BS—no competing interests. RW—no competing interests. ML—no competing interests. AZ—no competing interests. TG—no competing interests.

Author details

[1]Institute of Geoscience, Division of Geochemistry and Petrology, University of Bonn, Meckenheimer Allee 169, 53115 Bonn, Germany. [2]Centre for Rock Art Research and Management, University of Western Australia, Perth, WA 6009, Australia. [3]CNRS UMR 5199 PACEA, Université de Bordeaux, Bât B2, Allée Geoffroy Saint-Hilaire CS 50023, 33615 Pessac Cedex, France. [4]Rock Art Research Institute, GAES, University of the Witwatersrand, P. Bag 3, P.O. Wits, Johannesburg 2050, South Africa. [5]Institut für Evolutionsbiologie und Ökologie, University of Bonn, An der Immenburg 1, 53121 Bonn, Germany.

Received: 22 February 2022 Accepted: 22 April 2022
Published online: 09 June 2022

References

1. Donaldson M. Understanding the Rocks: Rock Art and the Geology of Murujuga (Burrup Peninsula). Rock Art Res. 2011;28(1):35.
2. Bird, C, Hallam SJ. A review of archaeology and rock art in the Dampier Archipelago. A report prepared for the National Trust of Australia (WA). 2006.
3. Mulvaney K. About time: toward a sequencing of the Dampier Archipelago petroglyphs of the Pilbara region, Western Australia. Rec West Aust Mus Sup. 2011;79:30–49.
4. Mulvaney K. Murujuga Marni: rock art of the macropod hunters and mollusc harvesters. Apollo Books. Perth: UWA Publishing; 2015.
5. UNESCO. https://whc.unesco.org/en/tentativelists/6445/. Accessed 28 Jan 2022.
6. Wingate MTD. Ion microprobe geochronology of baddeleyite and the use of mafic dyke swarms in testing Precambrian continental reconstructions. Unpubl PhD thesis, Australian National University, Canberra. 1997.
7. Gleeson DB, Leopold M, Smith B, Black JL. Rock-art microbiome: influences on long term preservation of historic and culturally important engravings. Microbiol Aust. 2018;39(1):33–6.
8. Black JL, MacLeod ID, Smith BW. Theoretical effects of industrial emissions on colour change at rock art sites on Burrup Peninsula, Western Australia. J Archaeol Sci Rep. 2017;12:457–62.
9. Potter RM, Rossman GR. The manganese-and iron-oxide mineralogy of desert varnish. Chem Geol. 1979;25(1–2):79–94.
10. Dorn RI. Anthropogenic interactions with rock varnish. In: Dontsova K, Balogh-Brunstad Z, Roux GL, editors. Biogeochemical cycles: ecological drivers and environmental impact, geophysical monograph. Hoboken: American Geophysical Union and John Wiley and Sons Inc; 2020. p. 267–83.
11. Goldsmith Y, Stein M, Enzel Y. From dust to varnish: Geochemical constraints on rock varnish formation in the Negev Desert. Israel Geochim Cosmochim Acta. 2014;126:97–111.
12. Krinsley DH, DiGregorio B, Dorn RI, Razink J, Fisher R. Mn-Fe-enhancing budding bacteria in century-old rock varnish, Erie Barge Canal. New York J Geol. 2017;125(3):317–36.

13. Krumbein WE, Jens K. Biogenic rock varnishes of the Negev Desert (Israel) an ecological study of iron and manganese transformation by cyanobacteria and fungi. Oecologia. 1981;50(1):25–38.
14. Lingappa UF, Yeager CM, Sharma A, Lanza NL, Morales DP, Xi G, et al. An ecophysiological explanation for manganese enrichment in rock varnish. Proc Nat Acad Sci. 2021;118(25):e2025188118.
15. Pillans B, Fifield LK. Erosion rates and weathering history of rock surfaces associated with Aboriginal rock art engravings (petroglyphs) on Burrup Peninsula, Western Australia, from cosmogenic nuclide measurements. Quat Sci Rev. 2013;69:98–106.
16. Black JL. Perdaman Chemicals and Fertilisers PTY LYD Environmental Scoping Document Public Review. Submission to Western Australian Environmental Protection Authority. 2019.
17. Wright BJ. Dampier Archipelago Aboriginal sites. Unpubl report for incorporation into the Pilbara Study Report, WA Museum, Perth. 1974.
18. Bednarik RG. The survival of the Murujuga (Burrup) petroglyphs. Rock Art Res. 2002;19(1):29–40.
19. Lau D, Ramanaidou E, Furman S, Cole I, Hughes T, Hoobin, P. Field Studies of Rock Art Appearance—Final Report: Fumigation and Dust Deposition - Progress Report: Colour Change and Spectral Mineralogy. CSIRO Division of Exploration and Mining, Western Australia. 2007.
20. Black JL, Box I, Diffey S. Inadequacies of research used to monitor change to rock art and regulate industry on Murujuga (Burrup Peninsula) Australia. Rock Art Res. 2017;34(2):P130-148.
21. Gillett R. Burrup Peninsula air pollution study: report for 2004/2005 and 2007/2008. Department of Environment and Conservation, Western Australia. 2008.
22. Markley T, Wells M, Ramanaidou E, Lau D, Alexander D. Burrup Peninsula Aboriginal Petroglyphs: Colour Changes & Spectral Mineralogy 2004–2014. CSIRO Report. 2015.
23. Department of the Environment and Energy. National Pollutant Inventory. http://www.npi.gov.au/npidata. Accessed 28 Jan 2022.
24. Smith BW, Black JL, Hœrlé S, Ferland MA, Diffey SM, Neumann JT, Geisler T. The impact of industrial pollution on the rock art of Murujuga Western Australia. Rock Art Res. 2022;39(1):3–14.
25. Norton SA, Veselý J. Acidification and acid rain. In: Holland HD, Turekian KK, editors. Treatise on geochemistry. Elsevier: Pergamon; 2003.
26. Osborn HB, Cooper LR, Billings J. Rainwater quality in southeastern Arizona rangelands. USDA – AEA Southwest Rangeland Watershed Research Centre. 1981. https://repository.arizona.edu/handle/10150/301257. Accessed 11 April 2022.
27. Bednarik RG. The science of Dampier rock art [Series of parts]: part 1. Rock Art Res. 2007;24(2):209–46.
28. Majima H, Awakura Y, Mishima T. The leaching of hematite in acid solutions. Metall Mater Trans. 1985;16(1):23–30.
29. Schwertmann U. Solubility and dissolution of iron oxides. Plant Soil. 1991;130(1):1–25.
30. International Federation of Rock Art Organizations. Save Dampier rock art. http://www.ifrao.com/save-dampier-rock-art/. Accessed 28 Jan 2022.
31. The Guardian. Australia lodges world heritage submission for 50,000-year-old Burrup Peninsula rock art. https://www.theguardian.com/artanddesign/2020/jan/29/australia-lodges-world-heritage-submission-for-50000-year-old-burrup-peninsula-rock-art. Accessed 28 Jan 2022.
32. MacLeod I, Fish W. Determining decay mechanisms on engraved rock art sites using pH, chloride ion and redox measurements with an assessment of the impact of cyclones, sea salt and nitrate ions on acidity. Paper presented to the ICOM-CC 19th Triennial Conference Preprints, Beijing, 17–21 May. 2021.
33. Přikryl R, Lokajíček T, Svobodová J, Weishauptová Z. Experimental weathering of marlstone from Přední Kopanina (Czech Republic)—historical building stone of Prague. Build Environ. 2003;38(9–10):1163–71.
34. Sitzia F, Lisci C, Mirão J. Accelerate ageing on building stone materials by simulating daily, seasonal thermo-hygrometric conditions and solar radiation of CSA Mediterranean climate. Const Build Mater. 2021;266: 121009.
35. Neumann J. Experimental weathering of Aboriginal rock art from Murujuga, Western Australia: A proof of concept study. Unpubl Master thesis, University of Bonn. 2021.
36. Australian Government, Bureau of Meteorology. Climate statistics Karratha Aero. http://www.bom.gov.au/climate/averages/tables/cw_004083_All.shtml#temperature. Accessed 28 Jan 2022.
37. Wunderground. Weather History for IWASPEGS2. https://www.wunderground.com/dashboard/pws/IWASPEGS2/table/2019-04-21/2019-04-21/monthly. Accessed 28 Jan 2022.
38. Konica Minolta. CR-410 Specifications. https://www5.konicaminolta.eu/de/messgeraete/produkte/farbmessung/chroma-meter/cr-400-410/technische-daten.html. Accessed 28 Jan 2022.
39. Sherman J. The theoretical derivation of fluorescent X-ray intensities from mixtures. Spectrochim Acta. 1955;7:283–306.
40. Oxford Instruments. X-MET7000 Series. https://www.bergeng.com/mm5/downloads/oxford/X-MET-General-Brochure-Nov2013.pdf. Accessed 28 Jan 2022.
41. Hauke K, Kehren J, Böhme N, Zimmer S, Geisler T. In situ hyperspectral Raman imaging: A new method to investigate sintering processes of ceramic material at high-temperature. Appl Sci. 2019;9(7):1310.
42. Downs RT. The RRUFF Project: an integrated study of the chemistry, crystallography, Raman and infrared spectroscopy of minerals. In Program and Abstracts of the 19th General Meeting of the International Mineralogical Association in Kobe, Japan. 2006.
43. Horiba. LabSpec 6 Spectroscopy Suite version 6. https://www.horiba.com/en_en/products/detail/action/show/Product/labspec-6-spectroscopy-suite-software-1843/. Accessed 28 Jan 2022.
44. Object Research Systems (ORS) Inc. Dragonfly version 2020.2.0.941. 2021.
45. Schindelin J, Arganda-Carreras I, Frise E, Kaynig V, Longair M, Pietzsch T, et al. Fiji: an open-source platform for biological-image analysis. Nat Meth. 2012;9(7):676–82.
46. Charola AE. Acid rain effects on stone monuments. J Chem Edu. 1987;64(5):436.
47. Homma Y, Kouketsu Y, Kagi H, Mikouchi T, Yabuta H. Raman spectroscopic thermometry of carbonaceous material in chondrites: four-band fitting analysis and expansion of lower temperature limit. J Min Petrol Sci. 2015;110:276–82. https://doi.org/10.2465/jmps.150713a.
48. Bednarik RG. Experimental colorimetric analysis of petroglyphs. Rock Art Res. 2009;26:55–64.
49. Smith BW, Black JL, Mulvaney KJ, Hoerlé S. Monitoring Rock Art Decay: Archival Image Analysis of Petroglyphs on Murujuga, Western Australia. Submitted: Conserv. Manag. Archaeol. Sites.
50. Parsons M, Johnson J, Guo J, Brashers B. Study of the cumulative impacts of air emissions in the Murujua airshed. *Ramboll Australia Pty Ltd.,* 2021. 41 St Georges Terrace, Perth, Western Australia 6000, Australia.

Publisher's Note